Novel high-entropy perovskite-type symmetrical electrode for efficient and durable carbon dioxide reduction reaction

Dong Zhang[a], Yao Wang[a,*], Yuhan Peng[a], Yao Luo[a], Tong Liu[b,*] Wei He[c], Fanglin Chen[d,*], Mingyue Ding[a,*]

[a] *Key Laboratory of Hydraulic Machinery Transients (Wuhan University), Ministry of Education, School of Power and Mechanical Engineering, Wuhan University, Wuhan, Hubei 430072, China.*

[b] *Key Laboratory of Green Chemical Process of Ministry of Education, Hubei Key Laboratory of Novel Reactor and Green Chemical Technology, School of Chemical Engineering and Pharmacy, Wuhan Institute of Technology, Wuhan 430205, China*

[c] *Jiangsu Key Laboratory of Advanced Metallic Materials, School of Materials Science and Engineering, Southeast University, Nanjing, Jiangsu 211189, China*

[d] *Department of Mechanical Engineering, University of South Carolina, Columbia, South Carolina 29208, United States*

[*]Corresponding author.

E-mail address: pmewy@whu.edu.cn (Y. W.), liu_tong@wit.edu.cn (T. L.), chenfa@cec.sc.edu (F. C.), & dingmy@whu.edu.cn (M. D.)

Abstract

Excessive emission of carbon dioxide (CO_2) has posed an imminent threat to human's environment and global prosperity. To achieve a sustainable future, solid oxide electrolysis cell (SOEC), which can efficiently combine CO_2 reduction reaction (CO_2RR) and renewable energy storage, has become increasingly attractive owing to its unique functionalities. Additionally,

symmetrical SOEC (SSOEC) has been considered as one of the most versatile cell configurations due to its simplified process, high compatibility and low cost. However, the electrode material requirements become very demanding since efficient catalytic-activities are required for both CO_2RR and oxygen evolution reaction (OER). Herein, we demonstrate a novel high-entropy perovskite type symmetrical electrode $Pr_{0.5}Ba_{0.5}Mn_{0.2}Fe_{0.2}Co_{0.2}Ni_{0.2}Cu_{0.2}O_{3-\delta}$ (HE-PBM) for SSOEC. B-site doping of transition metals such as Mn, Fe, Co, Ni, and Cu in HE-PBM anode has been found to strongly accelerate the OER in the anode. Moreover, the presence of *in-situ* formed Fe-Co-Ni-Cu quaternary alloy nanocatalysts from HE-PBM cathode under reducing atmosphere has resulted in superior catalytic-activity towards CO_2RR. The faster kinetics are also reflected by the significantly low polarization resistance of 0.289 Ω cm^2 and high electrolysis current density of 1.21 A cm^{-2} for CO_2RR at 2.0 V and 800 °C. The excellent electrochemical performance and stability demonstrate that the high-entropy perovskite material is a promising electrode material in SSOEC for efficient and durable CO_2RR.

Keywords: High-entropy oxide; Carbon dioxide reduction reaction; Quaternary alloy; *In-situ* exsolution; Solid oxide electrolysis cell.

1. Introduction

Due to ever increasing global industrial activities and the extensive use of fossil fuels, CO_2 emissions are constantly increasing. The urgent economic and political problems of the world's countries have also shifted toward tackling the global warming. Converting atmospheric CO_2 into reusable chemical energy is an effective and sustainable way to slow the growth of CO_2 emissions and mitigate the greenhouse effect[1-3]. Among the existing methods, electrochemical CO_2 reduction reaction (CO_2RR) via a solid oxide electrolysis cell (SOEC) is an effective CO_2 conversion method, and electrocatalytic CO_2 conversion holds great promise as a future technology for long-term storage of renewable energy and sequestration of CO_2 in the earth's carbon cycle. In general, CO_2RR can be carried out over a wide range of temperatures and/or pressures, and therefore becomes a prominent research direction.

SOEC is an important tool for the increasingly widespread use of carbon dioxide resources owing to its unique functionalities[4-9]. The electricity used can be derived from intermittent energy sources such as wind, solar and tidal energy, thus storing electricity at the same time. Oxygen ions (O^{2-}) separated from CO_2 at intermediate temperatures can pass through the electrolyte of the oxide ionic conductor[10-13]. However, its high cost and complex assembly have severely hindered its practical application. A symmetrical solid oxide electrolysis cell (SSOEC), where the same electrode material is used on both sides of the cell, is an effective way of simplifying the production of the cell and lowering costs[14-18]. The current anode material and cathode material correspond to high performance oxygen evolution reactions (OER) and CO_2RR, respectively[19]. In contrast, the SSOEC is made of the same material as both anode and cathode. Therefore, the selection of appropriate materials with both good

electro-catalytic activity as well as stability towards OER and CO_2RR is key to its advancement.

In recent years, some perovskite materials have been investigated as electrodes for SSOECs, such as $Sr_2Fe_{1.5}Mo_{0.5}O_{6-\delta}$[20], $La_{0.75}Sr_{0.25}Cr_{0.5}Mn_{0.5}O_{3-\delta}$[21], and $Pr_{0.5}Ba_{0.5}MnO_{3-\delta}$[22]. In addition, some new materials such as $La_{0.8}Sr_{1.2}Fe_{0.9}Co_{0.1}O_{4-\delta}$[16] and $La_{0.3}Sr_{0.7}Fe_{0.7}Ti_{0.3}O_{3-\delta}$[23] have also been investigated for electrode in SSOECs. Among all these materials, $Pr_{0.5}Ba_{0.5}MnO_{3-\delta}$ (PBM) exhibits relatively high electrical conductivity, excellent redox stability, and coking tolerance. However, the development of suitable electrodes comparable in performance to conventional Ni-YSZ but more stable remains a challenge.

Recently, high-entropy oxide (HEO) was proposed, which showed excellent chemical properties due to the highly disordered structural features and a multi-component random distribution[24-29]. For instance, $La_{0.8}Sr_{0.2}MnO_{3-\delta}$ (LSM) has been employed as a high-entropy cathode with A-site or B-site doping in SOFC, which exhibits high performance and suppresses Sr segregation[30-32]. A $La_{0.2}Pr_{0.2}Nd_{0.2}Sm_{0.2}Ba_{0.1}Sr_{0.1}Co_{0.2}Fe_{0.6}Ni_{0.1}Cu_{0.1}O_{3-\delta}$ high entropy perovskite (HEP) with high elements contents was also proposed as a cathode for SOFC[33]. However, there have been no reports of high entropy perovskite materials as symmetrical electrodes in SSOECs. Currently, there are generally two definitions of HEO: one is composed of at least five elements (5%-35%) in the composition; the other is that the conformational entropy (S) needs to be higher than 1.5R (R is gas constant). The configurational entropy can be calculated with the formula of $S = - R\cdot\Sigma\, x_i\cdot\ln(x_i)$[34], where x_i is the mole percent of component *i*.

In this work, we design a symmetrical electrode of high-entropy perovskite oxide $Pr_{0.5}Ba_{0.5}Mn_{0.2}Fe_{0.2}Co_{0.2}Ni_{0.2}Cu_{0.2}O_{3-\delta}$ (HE-PBM) for CO_2 electrolysis via a SSOEC, and the

transition elements can promote OER in the anode, while the *in-situ* exsolved Co-Fe-Ni-Cu quaternary alloy nanoparticles can accelerate CO_2RR in the cathode. The configurational entropy of HE-PBM is 2.30R, which qualifies as HE oxides. Electrical and chemical properties of HE-PBM and traditional PBM were compared in symmetrical single cells, and the mechanism of the performance enhancement in high-entropy perovskite was proposed. This work offers an alternative symmetrical electrode in SSOEC applications.

2. Results and discussion

2.1. Phase composition and morphology

Fig. 1a shows the Rietveld refined X-ray diffraction (XRD) pattern of HE-PBM after the initial synthesis at 1100 °C. The well-fitting data show that all the peaks belong to a cubic structure without any impurity, and the lattice parameters of HE-PBM are a=b=c=3.884 Å. XRD of as-prepared PBM powder (Fig. S1) exhibits cubic and hexagonal mixed phases, in agreement with other reports [35]. High-resolution transmission electron microscopy (HR-TEM) images of HE-PBM in Fig. 1b-c show that the particle size is approximately 250-300 nm, and the lattice spacing of the crystal is measured to be 0.278 nm, consistent to the XRD result. Energy-dispersive X-ray spectroscopy (EDS) element mapping in Fig. 1d shows that all the elements involving Pr, Ba, Mn, Fe, Co, Ni, Cu, and O elements are uniformly distributed on the surface of the HE-PBM, indicating that all the metal ions are successfully integrated into the lattice. It is well-known that Goldschmidt tolerance factor (t) is a key-parameter to evaluate the degree of structure distortion based on the geometric configuration and ionic radii according to Eq. (1):

$$t = \frac{r_A + r_O}{\sqrt{2}(r_B + r_O)} \quad (1)$$

where r_A, r_B and r_O represent the radii of A-site, B-site and oxygen-ion in the perovskite material, respectively. The Goldschmidt tolerance factor (t) of the HE-PBM is calculated to be 0.88, which is located in the range of $0.78 < t < 1.05$, further indicating that this high-entropy oxide belongs to a perovskite [30, 31, 36]. The schematic diagram of the crystal structure is shown in Fig. 1e. The chemical compatibility between HE-PBM and LSGM electrolyte was also examined by the XRD, and the results are shown in Fig. S2 indicate that no secondary phase has been formed during the sintering process up to 1000 °C[37-39].

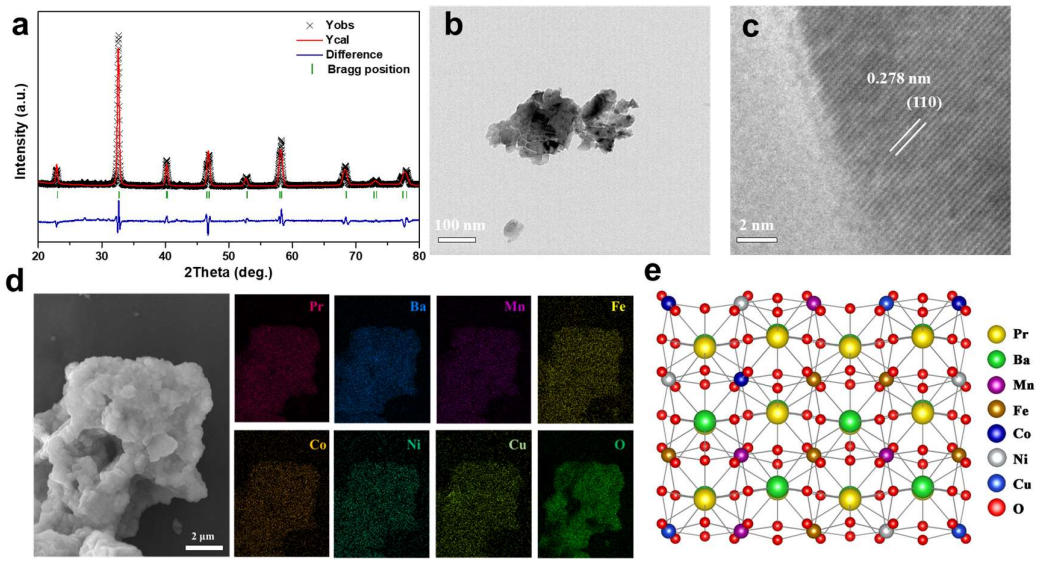

Fig. 1. (a) Powder XRD patterns for the synthesized PBM and HE-PBM powders, (b) TEM and (c) HR-TEM images for HE-PBM, (d) SEM image and EDS element distribution diagram of HE-PBM, (e) The schematic diagram of HE-PBM crystal structure.

2.2. Physicochemical properties

As electrodes for SSOEC, sufficient catalytic activity is required for both electrode reactions, including OER in the anode and CO_2RR in the cathode. Thermogravimetric analysis (TGA) measurements were performed and shown in Fig. S3a to evaluate the oxygen non-stoichiometry.

The weight loss below 400 ºC corresponds to the evaporation of water and other gases adsorbed in powders. At temperatures above 400 ºC, the weight loss is probably attributed to the loss of lattice oxygen. Up to 850 ºC, HE-PBM powders exhibit a weight loss of 3.488%, higher than 1.576% for PBM, indicating a higher content of oxygen vacancies in HE-PBM. CO_2 adsorption and desorption properties are also evaluated for the electrode, as shown from the CO_2-temperature-programmed desorption (CO_2-TPD) curves in Fig. S3b. The peaks at 300-500 ºC are related to the decomposition of bidentate carbonates [40, 41], while the peak starting at 600 ºC corresponds to the chemical adsorption of CO_2, which dominates the binding capacity of CO_2[42]. The bonding of adsorbed CO_2 has efficiently reinforced as the temperature increases. The peaks of HE-PBM are higher than the PBM, indicating more favorable CO_2 adsorption in HE-PBM, which is beneficial to CO_2RR.

2.3. Nanoparticles generation in CO-CO_2

During the CO_2RR process, CO_2 has been converted to produce CO, which could reduce the electrode and alter its composition. The evolution of the HE-PBM was studied after treating it in the 67%CO-33%CO_2 atmosphere at 800 ºC. As shown from the scanning electron microscopy (SEM) images in Fig. 2a, nanoparticles were exsolved on the surface of the substrate. To evaluate the possibility of metal formation, the change of Gibbs free energy (ΔG) was calculated by using HSC6.0 software for the chemical reaction between Fe, Co, Ni, Mn, and Cu oxides with CO. The results show that ΔG is negative for reducing Fe, Co, Ni, and Cu oxides at 800 ºC (Eqs. 2-5), indicating that these four metals could be spontaneously generated after reduction in the CO atmosphere. For the Mn element, ΔG is negative when MnO_2 is reduced to Mn_2O_3 (-217.4 kJ mol^{-1}) but positive when Mn_2O_3 is reduced to Mn^0 (114.4 kJ mol^{-}

[1]), indicating that it is only thermodynamically favorable to reduce Mn^{4+} to Mn^{3+} with CO (Eq. 6) at 800 °C.

$$Fe_2O_3+3CO(g) \rightarrow 2\,Fe + 3CO_2(g), \quad \Delta G = -26.456\ kJ\ mol^{-1} \tag{2}$$

$$CoO+CO(g) \rightarrow Co + CO_2(g), \quad \Delta G = -30.752\ kJ\ mol^{-1} \tag{3}$$

$$NiO+CO(g) \rightarrow Ni + CO_2(g), \quad \Delta G = -46.972\ kJ\ mol^{-1} \tag{4}$$

$$CuO+CO(g) \rightarrow Cu + CO_2(g), \quad \Delta G = -129.084\ kJ\ mol^{-1} \tag{5}$$

$$Mn_2O_3+3CO(g) \rightarrow 2Mn + 3CO_2(g), \quad \Delta G = 114.363\ kJ\ mol^{-1} \tag{6}$$

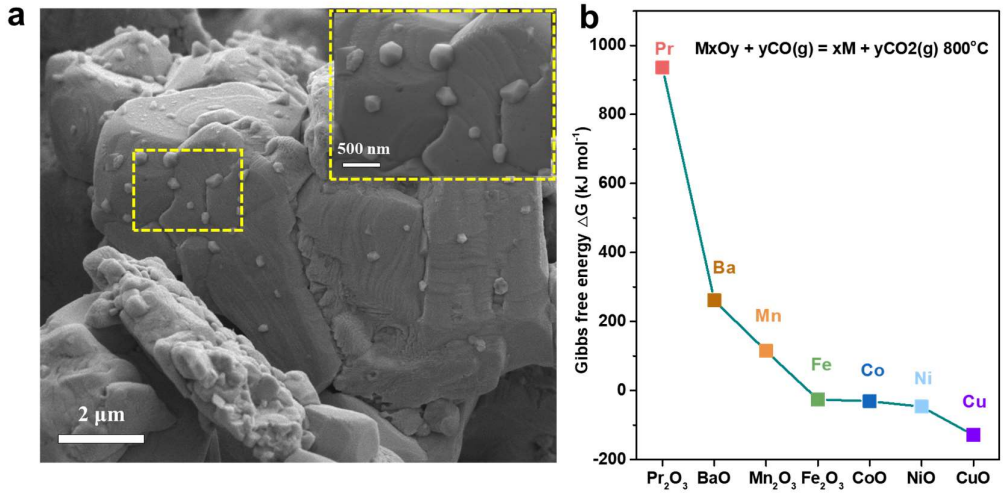

Fig. 2. (a) SEM image of reduced HE-PBM powders (b) The change of Gibbs free energy for the chemical reaction between Pr, Ba, Mn, Fe, Co, Ni, and Cu oxides with CO.

Fig. 3 shows HRTEM images of the reduced HE-PBM sample after being heat-treated in the CO-CO_2 atmosphere. Numerous nanoparticles with diameters of 10-40 nm have been exsolved from the substrate. Magnification of the nano-sized particles in Fig. 3b-c exhibits that nearly 1/3 of the *in-situ* exsolved nanoparticles in the bottom are deeply anchored into the substrate. High-angle annular dark field-scanning transmission electron microscopy (HADDF-STEM)-EDS mapping elemental analysis shows that Co, Ni, and Cu elements enrich in the exsolved

nanoparticles (Fig. 3d), while Pr, Ba, and Mn elements are uniformly distributed throughout the substrate. No significant enrichment of the Fe element was observable in the element mapping due to low discriminant validity with the substrate. However, the element line-scanning across the exsolved nanoparticle in Fig. 3e contains all four elements, Fe, Co, Ni, and Cu, consistent to the prediction from the negative ΔG (Fig. 2), indicating that the exsolved particles are quaternary alloys. The HADDF-STEM-EDS mapping test with overlapped images was also performed (Fig. S4). It can be seen that Ni, Co, and Cu are enriched on the same particle. Although Fe elements are widely distributed on the surface, they are more concentrated in the alloyed region.

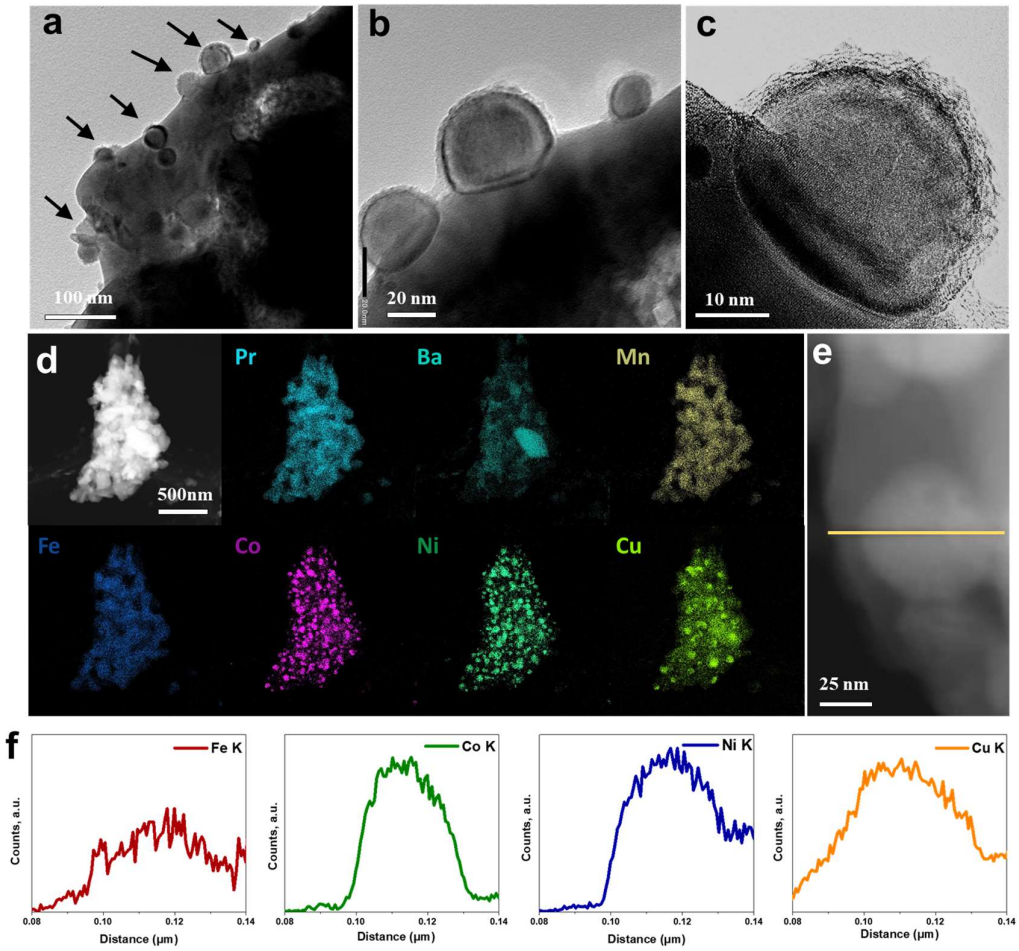

Fig. 3. (a)-(c) HRTEM image of reduced HE-PBM with exsolved nanoparticle at different

magnifications, (d) HADDF-STEM and EDS element mapping, (e)-(f) linear-scan images.

The valence states of fresh and reduced HE-PBM powders are measured by recording their X-ray photoelectron spectroscopy (XPS) spectra, and the results in the binding energy of 0-1000 eV are shown in Fig. S5. The fitting results of Fe 2p, Co 2p, Ni 2p, Cu 2p, Mn 2p, and O 1s spectra are present in Fig. 4a-e. The fitted result demonstrates that Fe^0, Ni^0, Co^0, and Cu^0 existed in the reduced HE-PBM (R-HE-PBM), confirming the exsolution of quaternary alloy[9, 43, 44]. These alloy nanoparticles can provide efficient active sites for the CO_2 reduction reaction. In the Mn 2p peaks, Mn^{4+} is the dominant chemical state in the fresh sample, and it converts to Mn^{4+} and Mn^{3+} in the R-HE-PBM sample, indicating that Mn is reduced in this process[30]. In the O 1s spectra (Fig. 4f), two characteristic peaks identified as lattice oxygen ($O_{lattice}$) in 529 eV and adsorbed oxygen (O_{ads}) in 531.1 eV are detected[40, 45]. The $O_{lattice}$ has been significantly decreased in the R-HE-PBM, implying that more oxygen vacancy is generated after reduction. The corresponding XPS fitting data with relative atomic concentration of Fe 2p, Co 2p, Ni 2p, Cu 2p, Mn 2p, and O 1s are listed in Table S1-S3.

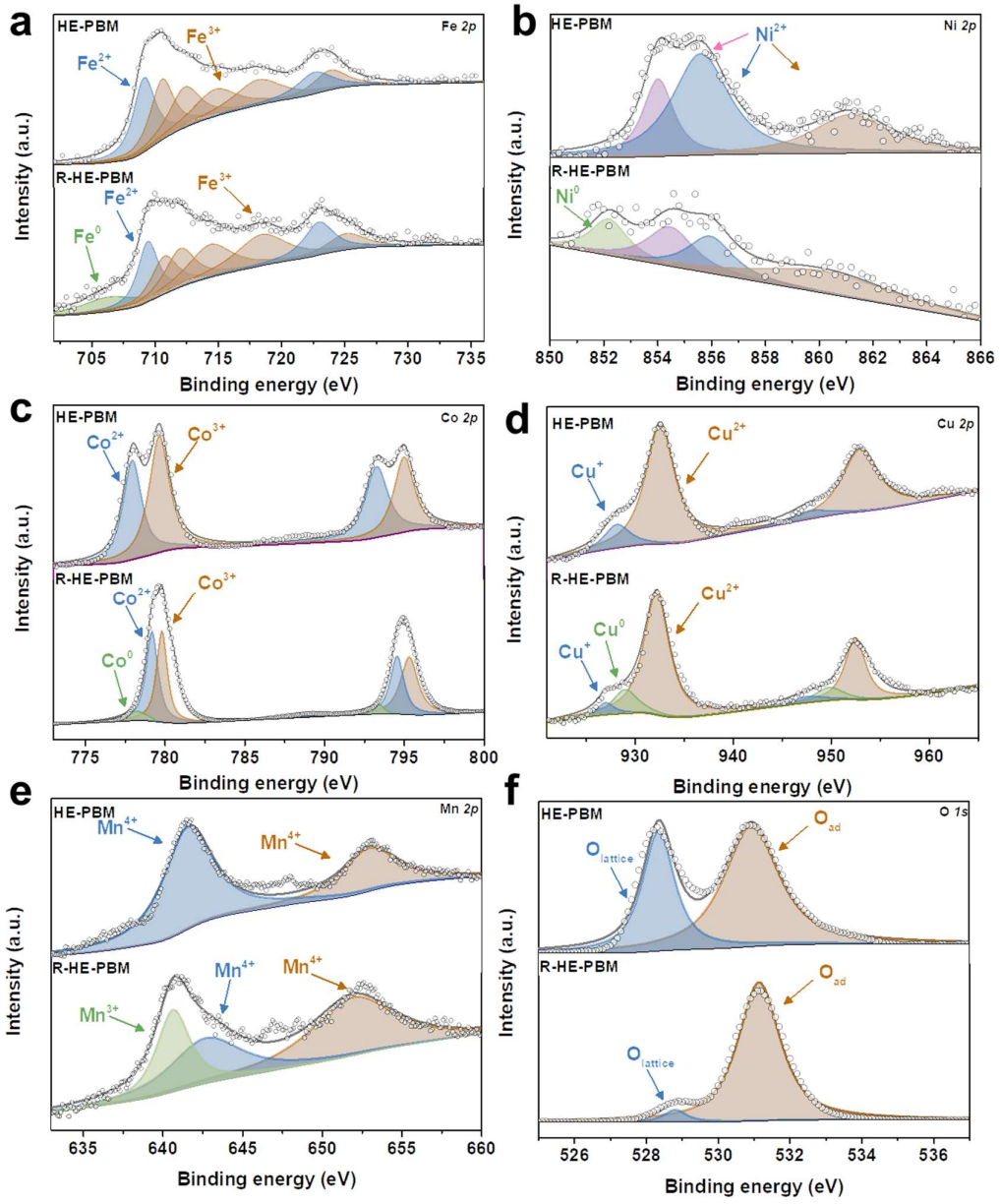

Fig. 4. XPS spectra of (a) Fe 2p, (b) Ni 2p, (c) Co 2p, (d) Cu 2p, (e) Mn 2p and (f) O 1s for HE-PBM before and after reduction treatment.

2.4. Electrochemical performance

The electrochemical performance of the LSGM electrolyte-supported solid oxide electrolyzers was carried out with PBM and HE-PBM as the symmetrical electrode. The cross-sectional morphology of the electrolyzer with the cell configuration of HE-PBM-SDC/LSGM/

HE-PBM-SDC is shown in Fig. S6. The electrolyzer consists of the ~20 μm-thick porous symmetrical cathode and anode, which are both well-connected to the dense LSGM electrolyte with a thickness of 250 μm.

Fig. 5a shows the electrochemical impedance spectra (EIS) measured at 800 °C under open circuit voltage (OCV) conditions and their corresponding fitting results by ZSimpWin software with an equivalent circuit of LR_{ohmic}(R1C1)(R2C2)(R3CPE3). Compared with PBM, the electrode polarization resistance (Rp=R1+R2+R3) of HE-PEM has significantly decreased from 0.808 to 0.291 Ωcm^2, indicating that the electrode reaction has been significantly accelerated. To further understand the electrode reaction process, distribution of relaxation times (DRT) method was used to separate the impedance spectra[46-49]. The peak in the DRT plots represents different sub-steps, and the integrated area represents each polarization resistance. As shown in Fig. 5b, the electrode reaction can be divided into three steps including a high-frequency step in 10^4-10^5 Hz, an intermediate frequency step in 10-10^4 Hz, and a low-frequency step in 1-10 Hz. In general, the high frequency (HF) region can be assigned to the O_2 evolution at the anode, the intermediate frequency (IF) region is mainly ascribed to the CO_2 electrochemical reduction process and carbonate intermediate species dissociation, and the low frequency (LF) region is associated to the surface exchange and O^{2-} transportation process [50, 51]. As shown from the DRT plot in Fig. 5b, the IF process is the predominant step, while both the IF and HF process has dramatically decreased in the HE-PBM electrode due to faster kinetics of electrode reaction. Fig. 5c shows the Arrhenius plot of the polarization resistance for PBM and HE-PBM, and an apparent activation energy (Ea) is decreased from 1.23 to 0.69 eV with a lower energy barrier. The corresponding Rp values are shown in the column graphs

(Fig. 5d).

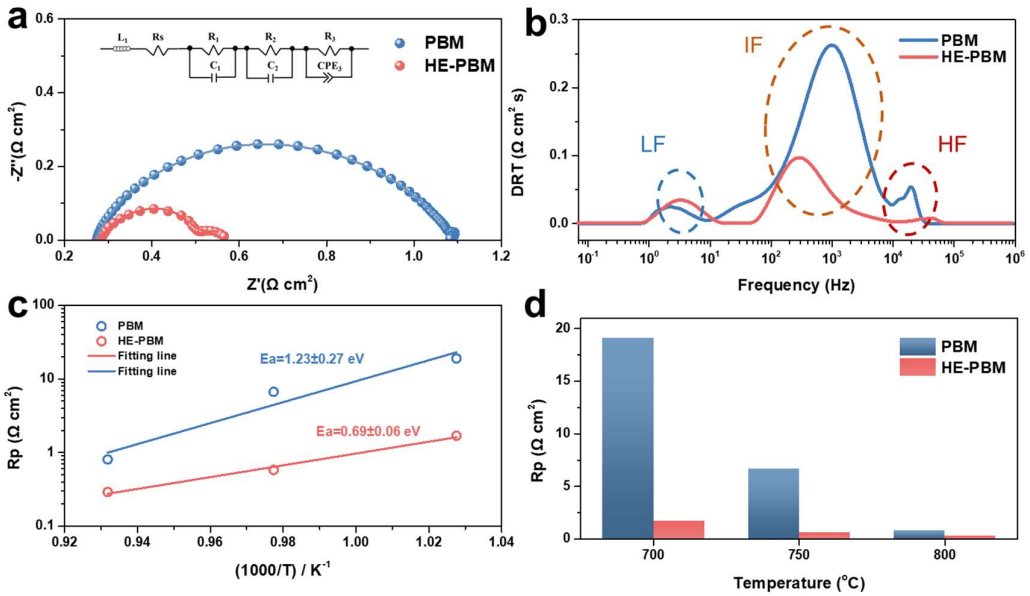

Fig. 5. (a) EIS data of the solid oxide electrolyzer of PBM and HE-PBM under OCV condition at 800 ºC, (b) the corresponding DRT analysis results of EIS data, (c) the Arrhenius plot of Rp in the temperature range of 700-800 ºC for PBM and HE-PBM, (d) the column graphs of Rp at different temperature.

The current density-voltage (*i-V*) curve with the applied voltage from OCV to 2.0 V is shown in Fig. 6a. The current density of PBM and HE-PBM symmetrical single cells reached 0.55 and 0.91 A cm^{-2} at 800 ºC and 2.0 V, respectively. Moreover, the electrochemical performance of the electrolyzer is significantly enhanced to 1.21 A cm^{-2} for the dual-phase HE-PBM-SDC ($Ce_{0.8}Sm_{0.2}O_{1.9}$) electrolyzer, which is 2.2 times higher than the PBM electrode. It can be noticed that the *i-V* curve shows a high linearity in the region of high voltage, which corresponds to the Tafel behavior in high polarization condition[52, 53]. As shown in Fig. 6b, Tafel plots of three electrodes with calculated slopes are given according to the Tafel equation (Supplementary Materials). It can be observed that the HE-PBMM-SDC electrode exhibits the lowest Tafel

slope value at the high voltage region, confirming the obtained excellent OER performance during the CO_2RR operation. Potentiostatic measurements at different voltages from 1.0 V to 1.6 V were conducted (Fig. 6c). The results are consistent with the *i-V* curve that the HE-PBM-SDC electrode exhibits a better electrochemical performance in CO_2RR. The corresponding CO production rate and Faraday efficiency on HE-PBM-SDC electrode are summarized in Fig. 6d. Faraday efficiency higher than 95% is obtained at the different applied voltages, verifying the highly efficient CO_2RR and energy conversion process. To further illustrate the better CO_2RR performance of dual-phase electrodes, the EIS data for HE-PBM and HE-PBM-SDC single cells exposed to pure dry CO_2 and operated at 800 °C under 1.2 V were also measured and then fitted by using ZSimpWin software. It is shown in Fig. 6e that the polarization resistance (Rp) decreased from 1.89 to 1.09 Ωcm^2 by adding the SDC phase. Similarly, to illustrate the origin of the enhanced electrochemical catalytic performance, the EIS spectra in Fig. 6f are analyzed using the DRT method. The low frequency (LF) arc, related to the surface exchange and O^{2-} transportation process, was significantly decreased in the HE-PBM-SDC cell. The enhancement of introducing SDC into HE-PBM is mainly due to the generation of more active sites for CO_2 adsorption.

Moreover, the stability of the single cells is an essential factor for the application of SOECs. Therefore, the long-term tests of these electrolysis cells at 1.2V under 800 °C were performed (Fig. 6g). The HE-PBM-SDC cell reached a higher current density and there was no significant decay for the three electrodes within 60 hours[54-56]. Post-test analysis of the cells also displayed an intact microstructure with no delamination between the electrode and electrolyte.

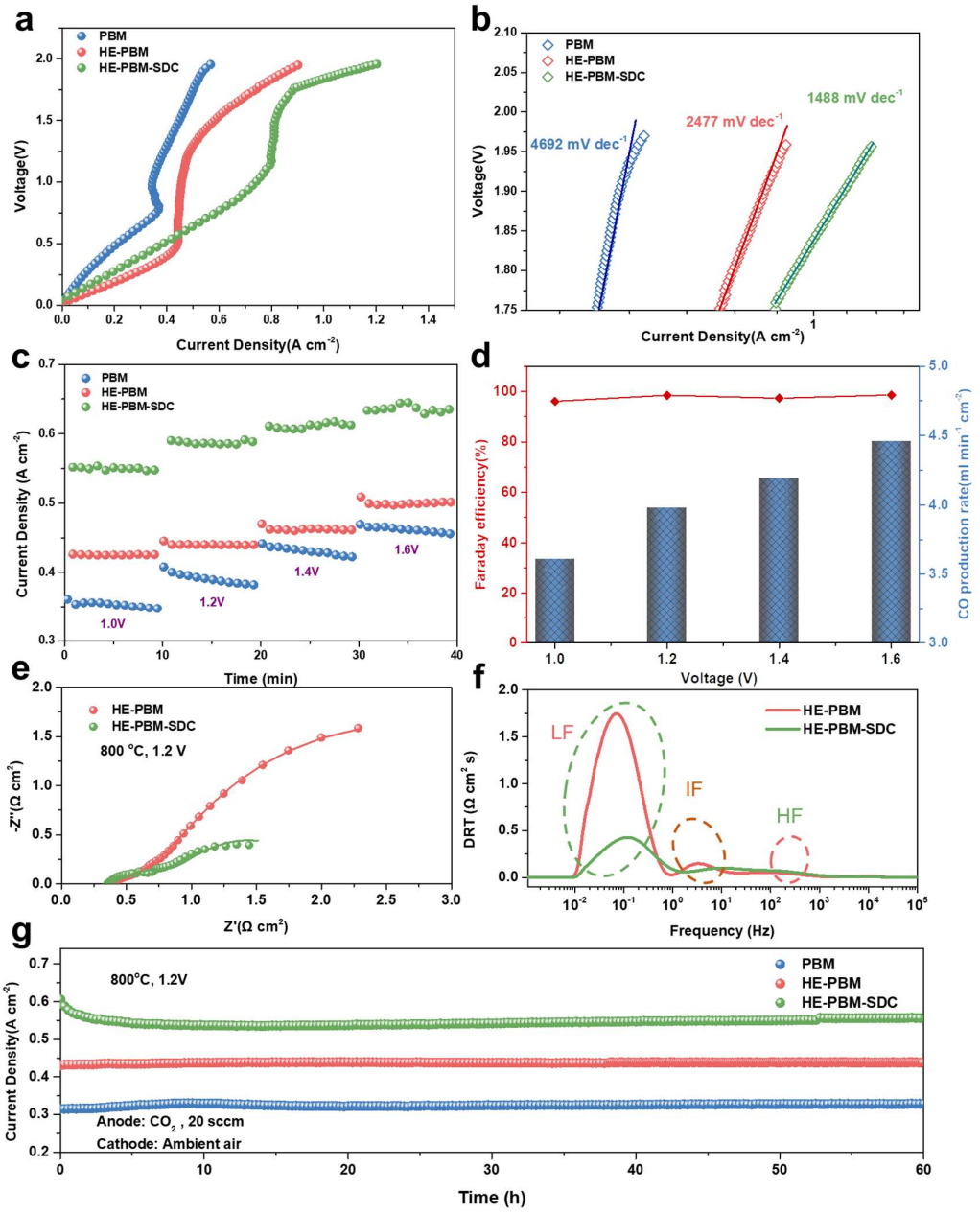

Fig. 6. (a) *i-V* curves for CO_2 electrolysis in the solid oxide electrolyzer with PBM, HE-PBM and HE-PBM-SDC electrode measured at 800 °C, (b) the corresponding Tafel curve in high current region with calculated Tafel slopes, (c) the potentiostatic tests for PBM, HE-PBM and HE-PBM-SDC electrodes of CO_2 electrolysis at different voltage at 800 °C, (d) Faraday efficiencies and CO production rates of HE-PBM-SDC electrode for CO_2 electrolysis at different applied potentials, (e) EIS spectra of HE-PBM and HE-PBM-SDC electrode at 1.2V, (f) the corresponding DRT analysis results of EIS data, and (g) long-term electrochemical stability during CO_2 electrolysis at 1.2V.

The microstructure of the HE-PBM-SDC electrode before and after the long-term test is shown in Fig. S7a-b. The fresh HE-PBM electrode reveals a smooth surface while abundant nanoparticles are exsolved and pined on the electrode surface after-test, which is consistent with the morphology in CO-CO_2 reduction. Furthermore, the ex-situ Raman spectrum was collected for the electrode before and after-test (Fig. S7c). and no signals belonging to carbon at 1340 and 1580 cm^{-1} were detected, indicating a good coking resistance [57]. Scheme 1 shows the diagram of the operation process of SSOEC with the reactions occurring at the high-entropy cathode and high-entropy anode, respectively. The presence of *in-situ* formed Fe-Co-Ni-Cu quaternary alloy nanocatalysts from HE-PBM cathode under reducing atmosphere has resulted in more active sites towards faster CO_2RR, while B-site doping of transition metals such as Mn, Fe, Co, Ni, and Cu in HE-PBM anode can serve as high-entropy catalyst to strongly accelerate the OER in the anode, making the whole system more efficient and energy-saving. These results fully illustrate the good stability of HE-PBM, offering a new option for electrode for SSOEC.

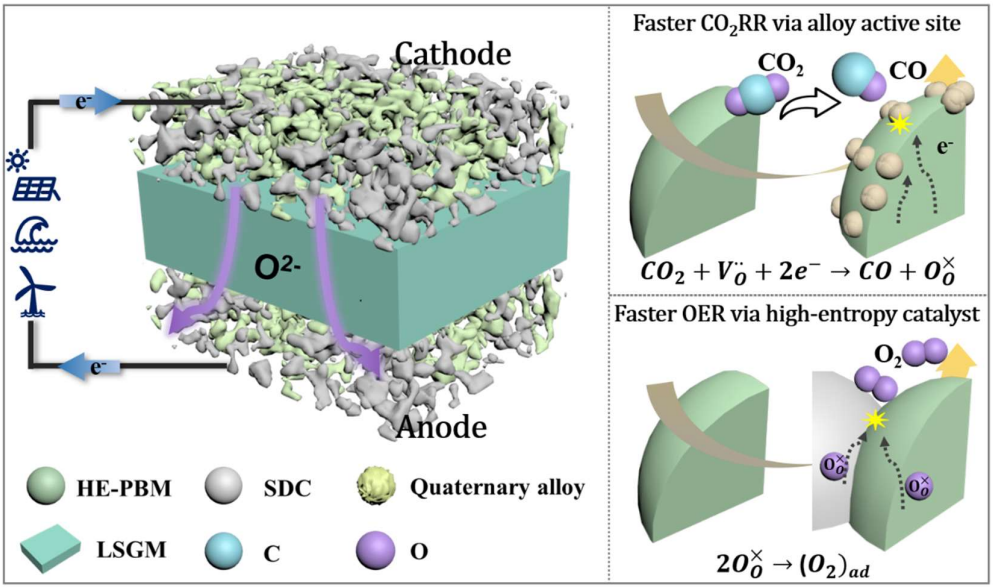

Scheme 1. The schematic of the evolution of quaternary alloy@HE-PBM-SDC in CO_2

electrolysis.

3. Conclusions

High entropy perovskite-type oxide HE-PBM was used as both the cathode and anode of a symmetrical solid oxide electrolyzer to perform CO_2 electrolysis. The HE-PBM cathode was reduced to exsolve multiple elements in random distribution and generate oxygen vacancies, which plays a significant role in enhancing the catalytic activity for CO_2RR. The electrolysis performance has been further increased in the composite by combining R-HE-PBM with SDC, and it exhibited a current density of 1.21 A cm^{-2} at 2 V and a low Rp of 1.09 Ωcm^2 at 800 °C. The electrode shows no decay or coking during the long-term operation. This work presents a promising way to design a symmetrical electrode with significant and stable performance.

4. Experimental

4.1. Powder synthesis

$Pr_{0.5}Ba_{0.5}Mn_{0.2}Fe_{0.2}Co_{0.2}Ni_{0.2}Cu_{0.2}O_{3-\delta}$ (HE-PBM) powders were synthesized via a sol−gel combustion route[35, 58, 59]. The SDC powder was synthesized via a combustion method. The synthesis process is listed in detail in the Supplementary Materials. The PBM electrode ink and HE-PBM ink are obtained by mixing the PBM powders or HE-PBM powders with α-terpineol (AR, Sinopharm Chemical Reagent Co., Ltd.) at a weight ratio of 10 : 15, while HE-PBM powders, $Ce_{0.8}Sm_{0.2}O_{1.9}$ (SDC) powders, and α-terpineol solution with a weight ratio of 7 : 3 : 15 are mixed to form the homogenous HE-PBM-SDC ink.

4.2. Characterization

The crystal structure of HE-PBM powders is investigated using XRD (Xpert Pro). The

element valence states of HE-PBM powders are examined by XPS (ESCALAB250Xi). The SEM and EDS-mapping of the HE-PBM electrode as well as the morphology of the symmetrical cell is measured via SEM (Tescan MIRA 3). HRTEM (JEM-F200) is used to determine the microstructures and fine structures of the samples. TGA of the pristine PBM and HE-PBM powders is carried out at the temperature range of 60-850 ºC by using a thermogravimetric analyzer (HTC-01, Hengjiu Instruments). CO_2-TPD is performed on a Micromeritics Chemisorption Analyzer (VODO VDsorb-91i) with a TCD detector. The coke deposition degree is evaluated by a Raman microscope (Renishaw RM-1000).

4.3. Cell preparation and Electrochemical measurements

Electrolyte-supported symmetrical single cells with a configuration of HE-PBM-SDC/LSGM/HE-PBM-SDC and PBM symmetrical cell was also prepared for comparison. Cell performance and polarization resistance were determined by an electrochemical workstation (Zahner Zennium E). EIS are collected at the temperature of 700-800 ºC with a voltage amplitude of 30 mV in the frequency range from 10 m to 1 M Hz, while *i-V* curves are measured from OCV to 2.0 V at a scan rate of 30 mV s^{-1}. The flow rate of feeding gas CO_2 in the cathodes is monitored by a digital mass flowmeter (APEX, Alicat Scientific) and set as 20 mL min^{-1}, while the anode is exposed to ambient air.

Acknowledgments

This work was supported by National Natural Science Foundation of China (U21A20317), the National Key Research and Development Program of China (2022YFA1504701), the Fundamental Research Funds for the Central University (2042022gf0002), the U.S. National Science Foundation (1832809) and the start-up research funds from Wuhan Institute of Technology (K202201). The authors also highly thank the Core Facility of Wuhan University

for XRD, XPS, Raman, and TEM analysis, and Large-scale Instrument & Equipment Sharing Foundation of Wuhan University.

References

[1]S. Gao, T. Wei, J. Sun, Q. Liu, D. Ma, W. Liu, S. Zhang, J. Luo, X. Liu, Atomically dispersed metal-based catalysts for Zn–CO_2 batteries, Small Struct. 3 (2022) 2200086, http://doi.org/10.1002/sstr.202200086

[2]C. Yin, Q. Li, J. Zheng, Y. Ni, H. Wu, A.-L. Kjøniksen, C. Liu, Y. Lei, Y. Zhang, Progress in regulating electronic structure strategies on Cu-based bimetallic catalysts for CO_2 reduction reaction, Adv. Powder Mater. 1 (2022) 100055, http://doi.org/10.1016/j.apmate.2022.100055

[3]Y. Tian, N. Abhishek, C. Yang, R. Yang, S. Choi, B. Chi, J. Pu, Y. Ling, J.T. Irvine, G. Kim, Progress and potential for symmetrical solid oxide electrolysis cells, Matter 5 (2022) 482-514, http://doi.org/10.1016/j.matt.2021.11.013

[4]Y. Zheng, J. Wang, B. Yu, W. Zhang, J. Chen, J. Qiao, J. Zhang, A review of high temperature co-electrolysis of H_2O and CO_2 to produce sustainable fuels using solid oxide electrolysis cells (SOECs): advanced materials and technology, Chem. Soc. Rev. 46 (2017) 1427-1463, http://doi.org/10.1039/C6CS00403B

[5]Y. Zheng, Z. Chen, J. Zhang, Solid oxide electrolysis of H_2O and CO_2 to produce hydrogen and low-carbon fuels, Electrochem. Energy Rev. 4 (2021) 508-517, http://doi.org/10.1007/s41918-021-00097-4

[6]Y. Wang, W. Li, L. Ma, W. Li, X. Liu, Degradation of solid oxide electrolysis cells:

Phenomena, mechanisms, and emerging mitigation strategies—A review, J. Mater. Sci. Technol. 55 (2020) 35-55, http://doi.org/doi.org/10.1016/j.jmst.2019.07.026

[7]K. Chen, S.P. Jiang, Materials degradation of solid oxide electrolysis cells, J. Electrochem. Soc. 163 (2016) F3070-F3083, http://doi.org/10.1149/2.0101611jes

[8]A.S. Reis Machado, M. Nunes da Ponte, CO_2 capture and electrochemical conversion, Curr. Opin. Green Sustain. Chem. 11 (2018) 86-90, http://doi.org/10.1016/j.cogsc.2018.05.009

[9]S. Zhai, H. Xie, B. Chen, M. Ni, A rational design of FeNi alloy nanoparticles and carbonate-decorated perovskite as a highly active and coke-resistant anode for solid oxide fuel cells, Chem. Eng. J. 430 (2022) 132615, http://doi.org/10.1016/j.cej.2021.132615

[10]T. Zhang, J.C. Bui, Z. Li, A.T. Bell, A.Z. Weber, J. Wu, Highly selective and productive reduction of carbon dioxide to multicarbon products via in situ CO management using segmented tandem electrodes, Nat. Catal. 5 (2022) 202-211, http://doi.org/10.1038/s41929-022-00751-0

[11]X. Wang, S. Liu, H. Zhang, S. Zhang, G. Meng, Q. Liu, Z. Sun, J. Luo, X. Liu, Polycrystalline SnS_x nanofilm enables CO_2 electroreduction to formate with high current density, Chem. Commun. 58 (2022) 7654-7657, http://doi.org/10.1039/d2cc01888h

[12]S. Zhan, W. Ding, Z. Sun, W. Li, T. Xu, S. Wang, M. Zhang, Polyurethane/perovskite quantum dot elastomer composite with high stability and self-repairable properties, Adv. Powder Mater. 1 (2022) 100036, http://doi.org/10.1016/j.apmate.2022.100036

[13]Y. Zeng, Q. Hu, M. Pan, K. Zhang, S. Grasso, C. Hu, Q. Feng, Investigation of double perovskites Sr_2SmNbO_6 and X_2CoNbO_6 (X=Sr,Ba) with SCAN functional and plus U correction, Adv. Powder Mater. 1 (2022) 100019,

http://doi.org/10.1016/j.apmate.2021.11.006

[14]Y. Zhang, H. Zhao, Z. Du, K. Świerczek, Y.J.C.o.M. Li, High-performance $SmBaMn_2O_{5+\delta}$ electrode for symmetrical solid oxide fuel cell, Chem. Mater. 31 (2019) 3784-3793, http://doi.org/10.1021/acs.chemmater.9b01012

[15]Y. Tian, L. Zhang, Y. Liu, L. Jia, J. Yang, B. Chi, J. Pu, J. Li, A self-recovering robust electrode for highly efficient CO_2 electrolysis in symmetrical solid oxide electrolysis cells, J. Mater. Chem. A 7 (2019) 6395-6400, http://doi.org/10.1039/C9TA00643E

[16]L. Fu, J. Zhou, J. Yang, Z. Lian, J. Wang, Y. Cheng, K. Wu, Exsolution of Cu nanoparticles in $(LaSr)_{0.9}Fe_{0.9}Cu_{0.1}O_4$ Ruddlesden-Popper oxide as symmetrical electrode for solid oxide cells, Appl. Surf. Sci. 511 (2020) 145525, http://doi.org/10.1016/j.apsusc.2020.145525

[17]S. Hou, K. Xie, Enhancing the performance of high-temperature H_2O/CO_2 co-electrolysis process on the solid oxide $Sr_2Fe_{1.6}Mo_{0.5}O_{6-\delta}$-SDC/LSGM/$Sr_2Fe_{1.5}Mo_{0.5}O_{6-\delta}$-SDC cell, Electrochim. Acta 301 (2019) 63-68, http://doi.org/10.1016/j.electacta.2019.01.164

[18]Q. Wang, X. Tong, S. Ricote, R. Sažinas, P.V. Hendriksen, M. Chen, Nano-$LaCoO_3$ infiltrated $BaZr_{0.8}Y_{0.2}O_3$− electrodes for steam splitting in protonic ceramic electrolysis cells, Adv. Powder Mater. 1 (2022) 100003, http://doi.org/10.1016/j.apmate.2021.09.003

[19]D. He, W. Ruan, J. Li, J. Ni, C. Ni, Heterogeneity in the Mo doped $La_{0.55}Sr_{0.45}FeO_3$ cathode for direct CO_2 electrolysis, Chem. Eng. J. 433 (2022) 133632, http://doi.org/10.1016/j.cej.2021.133632

[20]Q. Liu, X. Dong, G. Xiao, F. Zhao, F. Chen, A novel electrode material for symmetrical SOFCs, Adv. Mater. 22 (2010) 5478-5482, http://doi.org/10.1002/adma.201001044

[21]J.C. Ruiz-Morales, J. Canales-Vázquez, J. Peña-Martínez, D.M. López, P. Núñez, On the

simultaneous use of $La_{0.75}Sr_{0.25}C_{r0.5}Mn_{0.5}O_{3-\delta}$ as both anode and cathode material with improved microstructure in solid oxide fuel cells, Electrochim. Acta 52 (2006) 278-284, http://doi.org/10.1016/j.electacta.2006.05.006

[22]B. Hua, Y.-F. Sun, M. Li, N. Yan, J. Chen, Y.-Q. Zhang, Y. Zeng, B. Shalchi Amirkhiz, J.-L.J.C.o.M. Luo, Stabilizing double perovskite for effective bifunctional oxygen electrocatalysis in alkaline conditions, Chem. Mater. 29 (2017) 6228-6237, http://doi.org/10.1021/acs.chemmater.7b01114

[23]Z. Cao, B. Wei, J. Miao, Z. Wang, Z. Lü, W. Li, Y. Zhang, X. Huang, X. Zhu, Q. Feng, Efficient electrolysis of CO_2 in symmetrical solid oxide electrolysis cell with highly active $La_{0.3}Sr_{0.7}Fe_{0.7}Ti_{0.3}O_3$ electrode material, Electrochem. Commun. 69 (2016) 80-83, http://doi.org/10.1016/j.elecom.2016.06.008

[24]C. Oses, C. Toher, S. Curtarolo, High-entropy ceramics, Nat. Rev. Mater. 5 (2020) 295-309, http://doi.org/https://doi.org/10.1038/s41578-019-0170-8

[25]L. Tang, Y. Yang, H. Guo, Y. Wang, M. Wang, Z. Liu, G. Yang, X. Fu, Y. Luo, C. Jiang, Y. Zhao, Z. Shao, Y. Sun, High configuration entropy activated lattice oxygen for O_2 formation on perovskite electrocatalyst, Adv. Funct. Mater. 32 (2022) 2112157, http://doi.org/10.1002/adfm.202112157

[26]C.M. Rost, E. Sachet, T. Borman, A. Moballegh, E.C. Dickey, D. Hou, J.L. Jones, S. Curtarolo, J.P. Maria, Entropy-stabilized oxides, Nat. Commun. 6 (2015) 8485, http://doi.org/10.1038/ncomms9485

[27]Y. Xu, X. Xu, L. Bi, A high-entropy spinel ceramic oxide as the cathode for proton-conducting solid oxide fuel cells, J. Adv. Ceram. 11 (2022) 794-804,

http://doi.org/10.1007/s40145-022-0573-7

[28]Q. Zhang, S. Zhang, Y. Luo, Q. Liu, J. Luo, P.K. Chu, X. Liu, Preparation of high entropy alloys and application to catalytical water electrolysis, APL Mater. 10 (2022) 070701, http://doi.org/10.1063/5.0097479

[29]D. Zhang, Y. Chen, H. Vega, T. Feng, D. Yu, M. Everett, J. Neuefeind, K. An, R. Chen, J. Luo, Long- and short-range orders in 10-component compositionally complex ceramics, Adv. Powder Mater. 2 (2023) 100098, http://doi.org/10.1016/j.apmate.2022.100098

[30]Y. Yang, H. Bao, H. Ni, X. Ou, S. Wang, B. Lin, P. Feng, Y. Ling, A novel facile strategy to suppress Sr segregation for high-entropy stabilized $La_{0.8}Sr_{0.2}MnO_{3-\delta}$ cathode, J. Power Sources 482 (2021) 228959, http://doi.org/10.1016/j.jpowsour.2020.228959

[31]X. Han, Y. Yang, Y. Fan, H. Ni, Y. Guo, Y. Chen, X. Ou, Y. Ling, New approach to enhance Sr-free cathode performance by high-entropy multi-component transition metal coupling, Ceram. Int. 47 (2021) 17383-17390, http://doi.org/10.1016/j.ceramint.2021.03.052

[32]F. He, Y. Zhou, T. Hu, Y. Xu, M. Hou, F. Zhu, D. Liu, H. Zhang, K. Xu, M. Liu, Y. Chen, An efficient high-entropy perovskite-type air electrode for reversible oxygen reduction and water splitting in protonic ceramic cells, Adv. Mater. (2023) e2209469, http://doi.org/10.1002/adma.202209469

[33]Q. Yang, G. Wang, H. Wu, B.A. Beshiwork, D. Tian, S. Zhu, Y. Yang, X. Lu, Y. Ding, Y. Ling, Y. Chen, B. Lin, A high-entropy perovskite cathode for solid oxide fuel cells, J. Alloys Compd. 872 (2021) 159633, http://doi.org/10.1016/j.jallcom.2021.159633

[34]W. Tillmann, L. Wojarski, D. Stangier, M. Manka, C. Timmer, Application of the eutectic high entropy alloy $Nb_{0.73}CoCrFeNi_{2.1}$ for high temperature joints, Weld. World 64 (2020)

1597-1604, http://doi.org/10.1007/s40194-020-00944-w

[35]S. Sengodan, S. Choi, A. Jun, T.H. Shin, Y.W. Ju, H.Y. Jeong, J. Shin, J.T. Irvine, G. Kim, Layered oxygen-deficient double perovskite as an efficient and stable anode for direct hydrocarbon solid oxide fuel cells, Nat. Mater. 14 (2015) 205-209, http://doi.org/10.1038/nmat4166

[36]A. Sarkar, R. Djenadic, D. Wang, C. Hein, R. Kautenburger, O. Clemens, H. Hahn, Rare earth and transition metal based entropy stabilised perovskite type oxides, J. Eur. Ceram. Soc. 38 (2018) 2318-2327, http://doi.org/10.1016/j.jeurceramsoc.2017.12.058

[37]Z. Zhan, D.M. Bierschenk, J.S. Cronin, S.A. Barnett, A reduced temperature solid oxide fuel cell with nanostructured anodes, Energ. Environ. Sci. 4 (2011) 3951, http://doi.org/10.1039/c1ee01982a

[38]E. Di Bartolomeo, F. Basoli, I. Luisetto, S. Tuti, F. Zurlo, Z. Salehi, S. Licoccia, Ni and Ni-Co $La_{0.8}Sr_{0.2}Ga_{0.8}Mg_{0.2}O_{3-\delta}$ infiltrated cells in $H_2$and CH_4/CO_2 mixture, Appl. Catal., B.Environ 191 (2016) 1-7, http://doi.org/10.1016/j.apcatb.2016.03.010

[39]X. Zhang, Y. Tong, T. Liu, D. Zhang, N. Yu, J. Zhou, Y. Li, X.K. Gu, Y. Wang, Robust Ruddlesden-Popper phase $Sr_3Fe_{1.3}Mo_{0.5}Ni_{0.2}O_{7-\delta}$ decorated with in-situ exsolved Ni nanoparticles as an efficient anode for hydrocarbon fueled solid oxide fuel cells, SusMat 2 (2022) 487-501, http://doi.org/10.1002/sus2.58

[40]X. Zhang, Y. Song, F. Guan, Y. Zhou, H. Lv, G. Wang, X. Bao, Enhancing electrocatalytic CO_2 reduction in solid oxide electrolysis cell with $Ce_{0.9}Mn_{0.1}O_{2-\delta}$ nanoparticles-modified LSCM-GDC cathode, J. Catal. 359 (2018) 8-16, http://doi.org/10.1016/j.jcat.2017.12.027

[41]W. Feng, Y. Song, X. Zhang, H. Lv, Q. Liu, G. Wang, X. Bao, Platinum-decorated ceria

enhances CO_2 electroreduction in solid oxide electrolysis cells, ChemSusChem 13 (2020) 6290-6295, http://doi.org/10.1002/cssc.202001002

[42]J. Li, J. Hou, Y. Lu, Q. Wang, X. Xi, Y. Fan, X.-Z. Fu, J.-L. Luo, Ca-containing $Ba_{0.95}Ca_{0.05}Co_{0.4}Fe_{0.4}Zr_{0.1}Y_{0.1}O_{3-\delta}$ cathode with high CO_2-poisoning tolerance for proton-conducting solid oxide fuel cells, J. Power Sources 453 (2020) 227909, http://doi.org/10.1016/j.jpowsour.2020.227909

[43]J. Qiao, H. Chen, Z. Wang, W. Sun, H. Li, K. Sun, Enhancing the catalytic activity of $Y_{0.08}Sr_{0.92}TiO_{3-\delta}$ anodes through in situ Cu exsolution for direct carbon solid oxide fuel cells, Ind. Eng. Chem. Res. 59 (2020) 13105-13112, http://doi.org/10.1021/acs.iecr.0c02203

[44]H. Hu, M. Li, H. Min, X. Zhou, J. Li, X. Wang, Y. Lu, X. Ding, Enhancing the catalytic activity and coking tolerance of the perovskite anode for solid oxide fuel cells through in situ exsolution of Co-Fe nanoparticles, ACS Catal. 12 (2021) 828-836, http://doi.org/10.1021/acscatal.1c04807

[45]Z. Liu, D. Cheng, Y. Zhu, M. Liang, M. Yang, G. Yang, R. Ran, W. Wang, W. Zhou, Z. Shao, Robust bifunctional phosphorus-doped perovskite oxygen electrode for reversible proton ceramic electrochemical cells, Chem. Eng. J. 450 (2022) 137787, http://doi.org/10.1016/j.cej.2022.137787

[46]A. Hauch, A. Hagen, J. Hjelm, T. Ramos, Sulfur poisoning of SOFC anodes: effect of overpotential on long-term degradation, J. Electrochem. Soc. 161 (2014) F734-F743, http://doi.org/10.1149/2.080406jes

[47]T. Liu, H. Liu, X. Zhang, L. Lei, Y. Zhang, Z. Yuan, F. Chen, Y. Wang, A robust solid oxide

electrolyzer for highly efficient electrochemical reforming of methane and steam, J. Mater. Chem. A 7 (2019) 13550-13558, http://doi.org/10.1039/C9TA00467J

[48]M. Saccoccio, T.H. Wan, C. Chen, F.J.E.A. Ciucci, Optimal regularization in distribution of relaxation times applied to electrochemical impedance spectroscopy: ridge and lasso regression methods - a theoretical and rxperimental study, Electrochim. Acta 147 (2014) 470-482, http://doi.org/https://doi.org/10.1016/j.electacta.2014.09.058

[49]J. Li, X. Zhou, C. Wu, L. Zhao, B. Dong, S. Wang, B. Chi, Self-stabilized hybrid cathode for solid oxide fuel cell: A-site deficient perovskite coating as solid solution for strontium diffusion, Chem. Eng. J. 438 (2022) 135446, http://doi.org/10.1016/j.cej.2022.135446

[50]H. Lv, L. Lin, X. Zhang, D. Gao, Y. Song, Y. Zhou, Q. Liu, G. Wang, X. Bao, In situ exsolved $FeNi_3$ nanoparticles on nickel doped $Sr_2Fe_{1.5}Mo_{0.5}O_{6-\delta}$ perovskite for efficient electrochemical CO_2 reduction reaction, J. Mater. Chem. A 7 (2019) 11967-11975, http://doi.org/10.1039/c9ta03065d

[51]S. Hu, L. Zhang, L. Cai, Z. Cao, Q. Jiang, W. Yu, Y. Wu, X. Zhu, W. Yang, Iron stabilized 1/3 A-site deficient La–Ti–O perovskite cathodes for efficient CO_2 electroreduction, J. Mater. Chem. A 8 (2020) 21053-21061, http://doi.org/10.1039/d0ta08088h

[52]M. Li, B. Hua, J. Chen, Y. Zhong, J.-L. Luo, Charge transfer dynamics in RuO_2/perovskite nanohybrid for enhanced electrocatalysis in solid oxide electrolyzers, Nano Energy 57 (2019) 186-194, http://doi.org/10.1016/j.nanoen.2018.12.048

[53]S. Lee, S.H. Woo, T.H. Shin, J.T.S. Irvine, Pd and GDC Co-infiltrated LSCM cathode for high-temperature CO_2 electrolysis using solid oxide electrolysis cells, Chem. Eng. J. 420 (2021) 127706, http://doi.org/10.1016/j.cej.2020.127706

[54]Y. Zhou, Z. Zhou, Y. Song, X. Zhang, F. Guan, H. Lv, Q. Liu, S. Miao, G. Wang, X. Bao, Enhancing CO_2 electrolysis performance with vanadium-doped perovskite cathode in solid oxide electrolysis cell, Nano Energy 50 (2018) 43-51, http://doi.org/10.1016/j.nanoen.2018.04.054

[55]F. He, M. Hou, F. Zhu, D. Liu, H. Zhang, F. Yu, Y. Zhou, Y. Ding, M. Liu, Y. Chen, Building efficient and durable hetero-Interfaces on a perovskite-based electrode for electrochemical CO_2 reduction, Adv. Energy Mater. 12 (2022) 2202175, http://doi.org/10.1002/aenm.202202175

[56]W. Wang, Y. Tian, Y. Liu, N. Abhishek, Y. Li, B. Chi, J. Pu, Tailored Sr-Co-free perovskite oxide as an air electrode for high-performance reversible solid oxide cells, Sci. China Mater. 64 (2021) 1621-1631, http://doi.org/10.1007/s40843-020-1567-2

[57]K.S. Blinn, H. Abernathy, X. Li, M. Liu, L.A. Bottomley, M. Liu, Raman spectroscopic monitoring of carbon deposition on hydrocarbon-fed solid oxide fuel cell anodes, Energ. Environ. Sci. 5 (2012) 7913-7917, http://doi.org/10.1039/c2ee21499g

[58]S. Joo, O. Kwon, K. Kim, S. Kim, H. Kim, J. Shin, H.Y. Jeong, S. Sengodan, J.W. Han, G. Kim, Cation-swapped homogeneous nanoparticles in perovskite oxides for high power density, Nat. Commun. 10 (2019) 697, http://doi.org/10.1038/s41467-019-08624-0

[59]J. Zhu, W. Zhang, Y. Li, W. Yue, G. Geng, B. Yu, Enhancing CO_2 catalytic activation and direct electroreduction on in-situ exsolved Fe/MnO_x nanoparticles from $(Pr,Ba)_2Mn_{2-y}Fe_yO_{5+\delta}$ layered perovskites for SOEC cathodes, Appl. Catal., B.Environ 268 (2020) 118389, http://doi.org/10.1016/j.apcatb.2019.118389

Dong Zhang obtained his bachelor's degree in energy chemical engineering from Wuhan University at 2021, and is pursuing his master degree in energy power engineering supervised by Dr. Yao Wang in School of Power and Mechanical Engineering at Wuhan University. His work focuses on the advanced electrode of solid oxide electrolysis cell including the advanced materials and the microstructure design.

Dr. Yao Wang received her bachelor's degree in materials science and engineering from Beijing University of Chemical Engineering, China, in 2008. She obtained her PhD in material science from University of Science and Technology of China, China, in 2013. She then worked as a postdoctoral researcher at University of South Carolina. She joined in School of Power and Mechanical Engineering, Wuhan University as a lecturer in 2014, and then was promoted to be an associate professor at 2017. Her research interests are focused on solid oxide cells, high-temperature electrolysis and inorganic membranes.

Dr. Tong Liu obtained his bachelor's degree in materials science and engineering from Harbin Institute of Technology, China, in 2008. He received his PhD in material science from University of Science and Technology of China, China, in 2013. He then worked as a postdoctoral researcher at University of South Carolina. He joined in School of Power and Mechanical Engineering, Wuhan University as a lecturer in 2015, and then was promoted to be an associate professor at 2017. In 2022, he joined in the School of Chemical Engineering and Pharmacy at Wuhan Institute of Technology as an associate professor. He has a particular interest in solid state chemistry and membrane process.

Dr. Fanglin (Frank) Chen is currently a full Professor in the Department of Mechanical Engineering at University of South Carolina. Prior to joining the University in Fall 2007, he has spent six years as Senior Staff Engineer at United Technologies Research Center. He received a Bachelor's Degree in Chemistry (1992) from Anhui University, a Masters Degree in Materials Science and Engineering (1995) from University of Science and Technology of China, and a Ph.D in Materials Science and Engineering (2001) from Georgia Institute of Technology. His research interests are in the area of synthesis and characterization of novel materials for electrochemical and catalytic applications such as solid oxide cells, separation membranes, and supercapacitors.

Dr. Mingyue Ding received his bachelor's degree in chemistry from Wuhan University, in 2003. He obtained his PhD degree in industrial catalysis from Institute of Coal Chemistry, Chinese Academy of Sciences, in 2009. He joined in Guangzhou Institute of Energy Conversion, Chinese Academy of Sciences as an assistant researcher in 2009, and then was promoted to be a research fellow at 2014. In 2016, he joined in School of Power and Mechanical Engineering, Wuhan University as a professor. His research interests are focused on energy chemistry and material, and low carbon molecules catalytic conversion.